ELSEVIER

Chemical Engineering Journal 88 (2002) 151–161

Chemical Engineering Journal

www.elsevier.com/locate/cej

Characterizing particle aggregates in a high-density and high-flux CFB riser

S.V. Manyele, J.H. Pärssinen, J.-X. Zhu*

Department of Chemical and Biochemical Engineering, University of Western Ontario, London, Ont., Canada N6A 5B9

Received 25 June 2001; received in revised form 10 October 2001; accepted 15 November 2001

Abstract

Particle aggregates play an important role in the performance of circulating fluidized beds (CFBs). This paper presents a study on the aggregate properties in a high-flux and high-density riser (10 m high and 76.2 mm i.d.), based on the solids concentration measurements using a fiber optic probe. The gas velocities ranged from 5.5 to 10 m/s and solids circulation rate between 100 and 550 kg/m^2 s. Sensitivity analysis was first conducted to establish the optimum settings for determining cluster parameters. Aggregate properties (frequency, time fraction, existence time, average solids concentration and cluster vertical dimension) were established using transient solids concentration data, based on the results of the sensitivity analysis. These parameters revealed a strong dependence of the aggregate properties on operating conditions, local mean solids concentration, radial position and axial elevation.

Keywords: High-density riser; Concentration fiber optic probe; Cluster time fraction; Existence time; Cluster frequency

1. Introduction

The gas–solid flow in circulating fluidized beds (CFBs) is often characterized by the existence of dense particle clouds referred to as particle aggregates or clusters [1,2]. The major properties of particle aggregate include appearance frequency, size, velocity, solids fraction and existence time. These aggregates play a major role in flow development length, axial dispersion of solids and gas, radial distribution of solids, solids flow direction in the wall region and erosion and heat transfer at the wall, and thus affect the overall performance of a CFB riser. Particles form aggregates as a result of flow instability [3], energy minimization [4], and particle–wake interactions [5]. In low-density risers, aggregate size and frequency have been found to increase with decreasing gas velocity [6]. Depending on the size, shape and particle population in the particle aggregates, they could be referred to as clusters (several dozens of particles), particle strands or streamers (stripe shape and significantly bigger than a cluster), and particle sheets and swarms often spotted at the wall [2]. All these forms of particle aggregates are also collectively referred to as clusters [1,2]. Clusters are responsible for high slip velocities and pressure fluctuations and for the core–annulus flow development [7].

Due to the gas–particle and particle–particle interactions, clusters form and break quickly and continuously. Under dilute conditions (high gas velocity, U_g, and low solids flux, G_s), the solids concentration signals are more uniform but have high frequency fluctuations associated with the passage of fast flowing dilute phase. As G_s is increased, the signal trace shows prolonged peaks due to the passage of more clusters. Near the wall, the solids concentration is high and the local gas velocity is low, hence larger aggregates may form and exist for longer time. Even when G_s is kept below 200 kg/m^2 s with $U_g < 6.5$ m/s, vigorous refluxing of solids (down flow) along the wall have been observed and attributed partly to aggregate formation [8–11].

Few experimental studies on cluster properties have been reported [7,12–15]. Using dual capacitance probes to obtain simultaneous solids concentration signals at two close locations, cluster sizes and velocity have been identified in a CFB [14]. Visual images of individual particles and swarms have also been analyzed using high-speed imaging [2,16]. Other methods used include laser sheet imaging techniques [15,17], video camera fiber optic probe combination [18,19] and high-speed motion analyzing systems [20]. Another approach has been computer aided mathematical modeling of cluster properties [12,21–26].

However, all the former studies were conducted under low-flux (and low-density) conditions, with G_s less than 200 kg/m^2 s. In this study, significantly higher solids flux

* Corresponding author. Tel.: +1-519-661-3807; fax: +1-519-850-2441.
E-mail address: zhu@uwo.ca (J.-X. Zhu).

1385-8947/02/$ – see front matter
PII: S1385-8947(01)00299-6

Nomenclature

f_c	overall cluster frequency with existence time longer than 3 ms (Hz)
f_{c1}	cluster frequency with existence time shorter than 15 ms (Hz)
f_{c2}	cluster frequency with existence time longer than or equal to 15 ms (Hz)
f_s	sampling frequency for solid concentration signals (Hz)
F_c	cluster time fraction (%)
F'_c	first derivative of the cluster time fraction (%)
G_s	solids circulation rate (kg/m^2 s)
L_v	characteristic vertical size of clusters (m)
n	number of standard deviation above mean value, used to define critical solids concentration (–)
N_s	total number of solids concentration samples in a particular cluster (–)
U_g	superficial gas velocity (m/s)
Z	axial distance above distributor (m)

Greek symbols

ε_{mf}	mean voidage at minimum fluidization conditions (–)
ε_s	local mean solids concentration (–)
$\bar{\varepsilon}_{sc}$	cluster average solids concentration (–)
ε_{scr}	threshold solids concentration (–)
$\bar{\tau}_c$	mean existence time of clusters at a local position (ms)
$\tau_{c,min}$	minimum existence time of clusters based on N_s (ms)

(300–550 kg/m^2 s) was studied with gas velocity between 5.5 and 10 m/s. Lower flux operating conditions (8.0 m/s, 100 kg/m^2 s) were also studied for comparison. This work also takes a wider approach to study the aggregate properties showing the frequency, existence time, clustering time fraction and solids fraction in clusters on several axial/radial positions. In addition, sensitivity analysis is introduced in identifying the clusters from solid concentration signals. The information obtained from this study could be beneficial especially for industrial catalytic applications (such as FCC) operated under higher solid fluxes from 400 to 1200 kg/m^2 s [27].

2. Experimental setup

The particle aggregates were studied in a CFB system that consists of two 10 m long risers. Both risers (0.076 and 0.203 m i.d.) utilize the same downcomer (0.320 m i.d.). The solids circulating in the system were FCC catalyst with a mean diameter of 67 μm and a particle density of 1500 kg/m^3. For the current work the measurements were conducted only in the 76 mm i.d. riser. The humidity level of the air was controlled between 70 and 80% to eliminate the electrostatics in the system.

After passing a butterfly valve section the solids entered the riser bottom at the height of 0.17–0.25 m. After initial gas–solid mixing and rapid acceleration during the first meters the solids (and particle aggregates) headed towards the riser top, where the gas–solid suspensions passed the smooth exit into the three-cyclone separation section for solids collection, before entering in a bag filter for cleaning. From the bottom of the large capacity bag filter fine particles could be returned back into the downcomer where a device for measuring solids flow rate is located. This device sectioned the column into two halves using a vertical plate and with two half-butterfly valves fixed at the top and the bottom of one of the sections. By appropriately flipping over the two valves from one side to the other, solids circulated through the system can be accumulated in one side of the measuring section for a given time period to provide the solids circulation rate. More details of this setup can also be found in literature [28].

Solid concentration measurements were conducted with a reflective-type fiber optic concentration probe. The active area in the probe tip was approximately 2 mm × 2 mm, consisting of approximately 8000 emitting and receiving quartz fibers, each having a diameter of 15 μm. More details of this probe including its calibration procedure can be found in literature [29]. Measurements were taken on eight axial levels (Z = 0.98, 1.53, 2.73, 3.96, 5.13, 6.34, 8.74 and 9.42 m) and at 11 radial positions (r/R = 0.00, 0.16, 0.38, 0.50, 0.59, 0.67, 0.74, 0.81, 0.87, 0.92 and 0.98). The sampling time is 60 s at a frequency of 970 Hz or a sampling interval of 0.00103 s.

To estimate the cluster length, a five-fiber optic bundle velocity probe was used to measure the particle velocities. The five-fiber optic bundle consists of two light emitting fibers (B and D) and three light detecting fibers (A, C and E) arranged precisely in the same line. A particle flowing by the center point between any two neighboring fibers will produce a reflective signal to a detection fiber. By counting the time difference between the two signals from A–B and B–C (or C–D and D–E), the velocity of a particle passing along the array of the five fibers can be determined. Details of the five-fiber optic bundle probe have been previously presented [30]. The particle velocity was measured at the same locations as those for the solid concentration measurements, with a sampling time typically over 30 s and the amount of sampled particles over 2500.

3. Cluster identification

Cluster information in CFB risers and downers can be obtained from local instantaneous solid concentration signals [12–14]. Based on the traces of the solid concentrations, the following technical and analytical criteria were sug-

gested to identify clusters [13]: (1) the solids concentration inside the cluster must be significantly higher than the local time–mean solids concentration; (2) the perturbation caused by a cluster must exist for significantly longer time than the sampling time interval; (3) this perturbation must also be sensed by a sampling volume which has a characteristic length scale greater than one to two orders of particle diameter. In accordance to the first criterion, one needs to set an appropriate threshold or critical solids concentration, ε_{scr}, above which a cluster is considered to be present. This critical concentration may be expressed as n-times the standard deviation of the sampled signal over the local time–mean solids concentration. Based on their data, Soong et al. [13] suggested $n = 3.0$ while Tuzla et al. [31] used $n = 2.0$. However, the basis for their choice of n was not explained. For the second criterion, the minimum time interval for the perturbation to be considered as a cluster may be expressed in terms of the number of consecutive samples above the critical solids concentration, N_s. Again, this has not been elucidated in the literature. Because the sensitive probe tip (2 mm × 2 mm) is 30 times the average particle diameter, the third criterion is satisfied.

The cluster properties investigated in this study include: (1) the cluster time fraction, F_c, defined as the ratio of the sum of the cluster existence times to the total sampling time; (2) the cluster frequency, f_c, defined as the number of clusters detected per unit time; (3) the mean cluster existence time, τ_c, defined as the average time interval between the initial and final detection of the clusters; (4) the mean solids concentration in clusters, $\bar{\varepsilon}_{sc}$, determined by averaging all sampled solids concentration values in each cluster, followed by averaging for all clusters detected; (5) the average number of clusters detected at a local position, determined from the cluster frequency and the total sampling time. However, all above parameters are dependent on the proper identification of each cluster from the time series of the solids concentration data, which in turn is related to the values of both n and N_s.

To identify the optimal values for both n and N_s, a sensitivity analysis is first introduced to elucidate their effects on the cluster properties. Considering the cluster time fraction, F_c, as a sample parameter for the sensitivity analysis, an increase/decrease of n would raise/lower the set critical solids concentration ($\varepsilon_{scr} = \bar{\varepsilon}_{sc} + n\sigma(\tau_c)$) and therefore decrease/increase the resulting total cluster time fraction, F_c, over the time series studied. With lower n (and therefore ε_{scr}) values, some of the solids concentration signals representing particles in the dispersed particulate phase (outside the clusters) will be counted as those representing clusters, and vice versa. However, since there are more particles in the dispersed particulate phase than in the clusters, there tends to be a sharp decrease of F_c when the set ε_{scr} value (and the corresponding n value) is increased beyond the value that demarcate the particulate phase and the clusters. In other words, there should be a sharp drop of F_c with increasing n. The variations of F_c with n for some selected data series

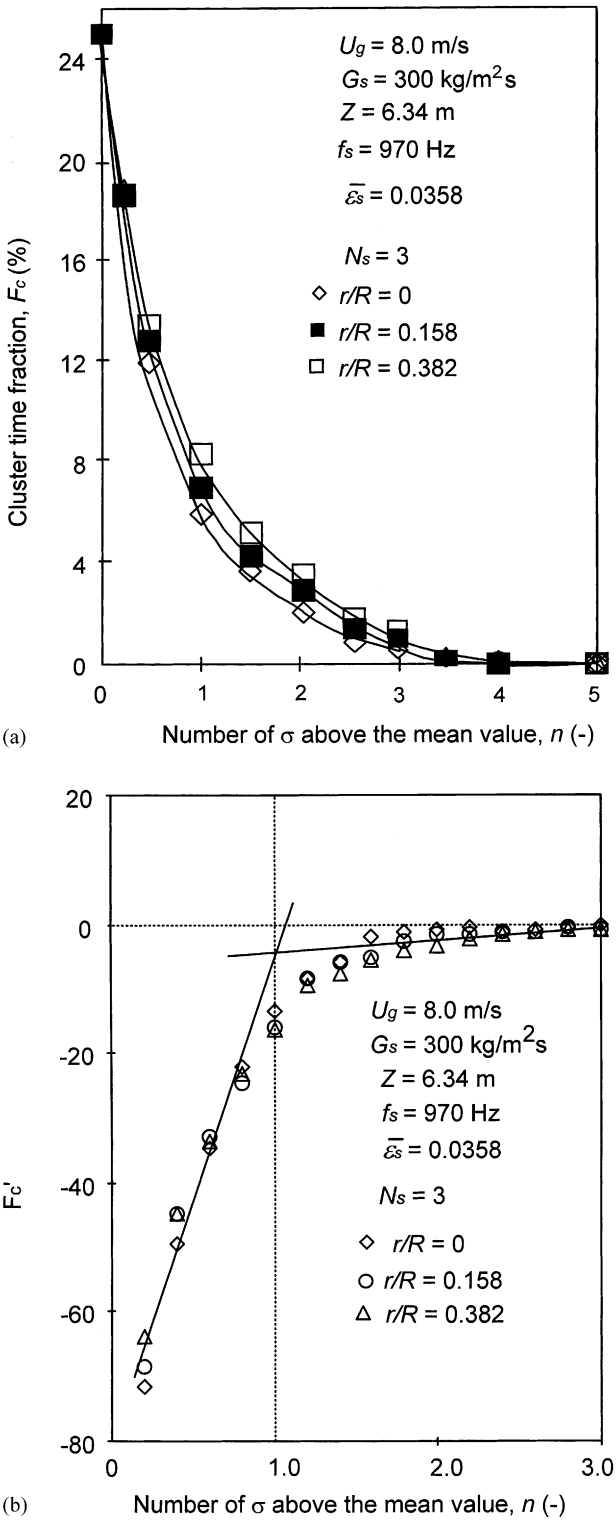

Fig. 1. (a) Variation of the cluster time fraction, F_c (%), with n for selected conditions at $U_g = 8.0$ m/s, $G_s = 300$ kg/m^2 s, $Z = 6.34$ m and $N_s = 3$. (b) Variation of the first derivative of the cluster time fraction, F_c (%), with n for selected conditions at $U_g = 8.0$ m/s, $G_s = 300$ kg/m^2 s, $Z = 6.34$ m and $N_s = 3$.

Table 1
Literature data on the values of n used in establishing cluster properties from solids concentration signal

	Author(s)		
	Soong et al. [13]	Tuzla et al. [31]	This work
n	3.0	2.0	1.0–1.4
N_s	Not given	Not given	3
F_c (%)	5–20	4–10	2–30
Measurement technique	Needle capacitance probe	Needle capacitance probe	Reflective fiber optic probe
Sampling frequency (Hz)	5000	5000	970
Operating conditions	$U_g = 5.0$ m/s, $G_s = 45$ kg/m^2 s	$U_g = 5$–6 m/s, $G_s = 89$ kg/m^2 s	$U_g = 5.5$–10 m/s, $G_s = 100$–550 kg/m^2 s

under high-flux conditions are plotted in Fig. 1(a) and the corresponding first derivatives, F_c', are plotted in Fig. 1(b). As shown there is a sharp change at $n = 1$. Similar analysis on the change of F_c versus N_s gives $N_s = 3$ as its optimal value.

It is worth noting that both optimal n and N_s values may vary with the operating conditions. For example, optimal n value was determined to be around 1.4 under low-flux ($G_s = 100$ kg/m^2 s). Therefore, different n values should be used for different conditions. In addition, it should also be understood that the cluster properties such as values of F_c thus obtained with the above method may not reflect 100% accurately the true values of those parameters given the nature of the data processing method. However, even information about their relative values are still of great interest in studying the particle aggregation behavior inside the CFB risers, especially those under high-flux operating conditions in comparison with low-flux operating conditions, since no such data is currently available. On the other hand as shown in Table 1, the results obtained in this study are comparable with those reported in the literature [13,14].

In this study, the mean cluster existence time has also been combined with average local particle velocity to estimate the average vertical cluster dimensions at different locations in the riser. Moreover, where the solids concentration is high, we limit the critical solids concentration to 40% to avoid exceeding the minimum fluidization solids concentration (58%).

4. Results and discussion

4.1. Solids distribution in the riser

The radial and axial distributions of solids in the risers have been widely studied and reported in the literature, especially for the low-flux risers. For high-flux risers, such studies are still few. Fig. 2 shows the radial profiles of the local mean solids concentration in our riser at four axial elevations and five high-flux operating conditions [28]. The profiles are similar to those found in low-flux risers, with high solids concentration near the wall and dilute core region, but with larger wall region. The bottom section is denser than the top section and the radial profiles flatten as the axial elevation increases. The effect of operating conditions in the core region is only appreciable at the bottom, while in the wall region the difference in operating conditions is more pronounced.

4.2. Cluster time fraction

Fig. 3 shows the radial profiles of F_c for different operating conditions at several axial elevations. F_c values are lower in the core than in the annular region, suggesting a severe particle aggregation in the annulus. This is understandable given the high solids concentration near the wall. The plot shows also that clusters exist for less than 10% of the time in the central region, but over 15–20% on average near the wall. Previously, it has been reported that clusters appear at

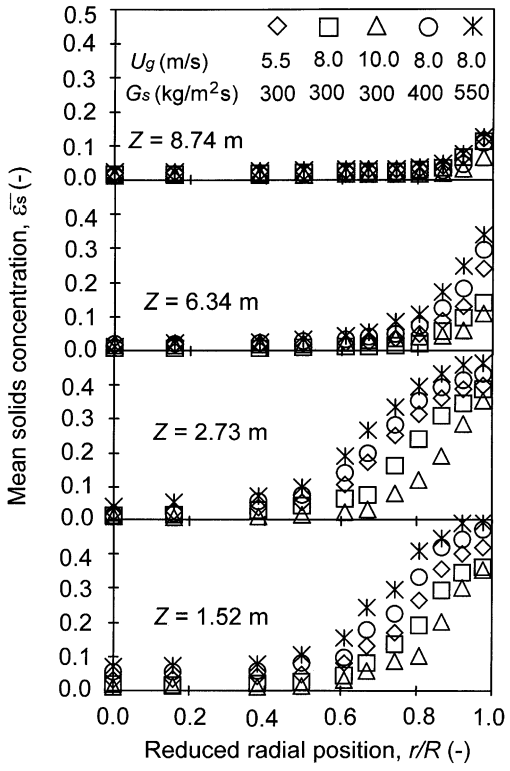

Fig. 2. Radial profiles of the time-averaged solids concentration at five different operating conditions and several axial elevations.

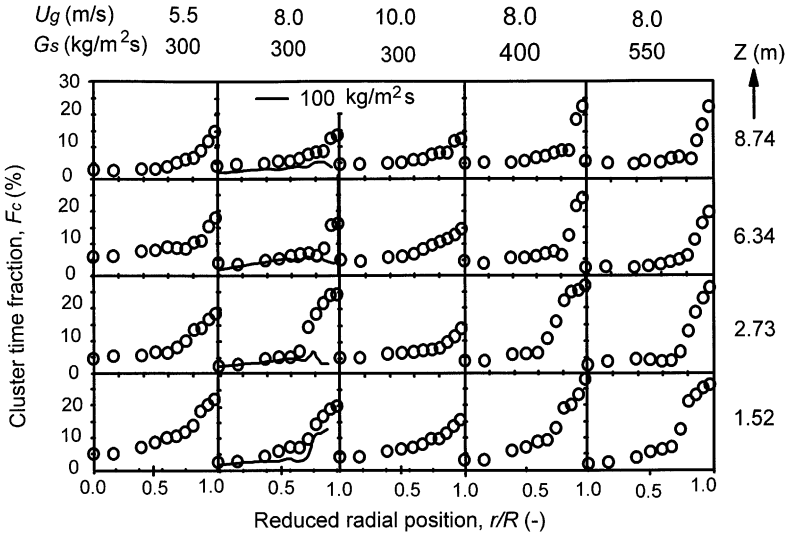

Fig. 3. Radial profiles of cluster time fraction for five different operating conditions and several axial elevations.

a maximum of 10% of time in risers, which however have been operated with low solids fluxes (and thus at fairly dilute conditions) [13,31]. This is in good agreement with our result in the more dilute riser center where clusters appeared typically for less than 10% of the time. Their results are also in good agreement with our data obtained under low-flux conditions ($G_s = 100\,kg/m^2\,s$) as shown by the solid curves in Fig. 3 for $U_g = 8.0\,m/s$ with all corresponding F_c values clearly less than 15%. In the core region, the values of F_c are comparable for low- and high-flux conditions. In the wall region however a major difference exists with high-flux condition leading to higher F_c values compared to low-flux conditions. Moreover for low-flux conditions, the radial profiles of F_c at the top of the riser are nearly flat while those at the bottom shows higher F_c values near the wall similar to high-flux conditions. At $U_g = 8.0\,m/s$ and $G_s = 100\,kg/m^2\,s$, maximum values of F_c reached up to 15% in the wall region of the bottom section, but only around 8% in the top section.

For all axial elevations, F_c increases towards the wall, but with different trend for different operating conditions. Increasing G_s makes such increase of F_c towards the wall more dramatic and increasing U_g makes such increase more gradual. These are inconsistent with the trend shown in Fig. 2, giving clear evidence that F_c depends on the local mean solids concentration. To further examine this dependency, F_c values obtained in the developed flow section ($Z = 6.34\,m$) are plotted versus the mean solids concentration for different local positions in Fig. 4. As shown, the cluster time fraction increases with increasing solids concentration, ε_s, for all operating conditions and axial elevations. Under the same ε_s, the gas velocity seems not to influence the cluster time fraction but an increased solids circulation rate slightly decreases the cluster time fraction. While the latter appears to be against the intuition, it is actually reasonable since the particles inside clusters would be more packed (see also Fig. 12 and the related discussion) under a high G_s so that the cluster time fraction would be smaller if ε_s is kept the same. Similarly, the cluster time fraction under low-flux conditions are comparably much higher, since the solids concentration inside the clusters are much lower (see also Fig. 12 and the related discussion). For all high-flux conditions, if neglecting the small variations due to the change with G_s, there appears

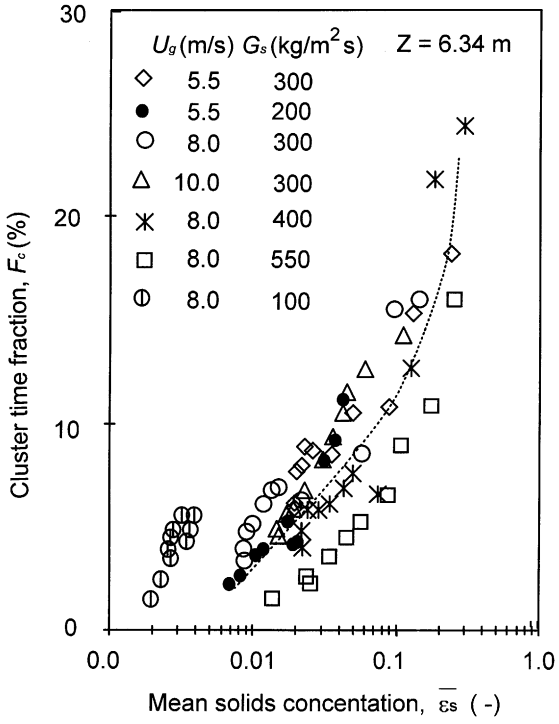

Fig. 4. Variation of local cluster time fraction with local mean solids concentration at different operating conditions and axial elevations.

to be a good correlation between the cluster time fraction and the mean solids concentration. For low-flux (more dilute) conditions, the span of the cluster time fraction is narrower showing that there are fewer clusters.

4.3. Cluster frequency

Because of the uneven distribution of solids in the high-flux riser, the cluster frequency also varies with both the location and the local mean solids concentration. The major factors affecting the cluster frequency are the cluster size and the local mean solids concentration, which changes with the operating conditions, the axial elevation from the distributor and the radial distance from the riser center. When large clusters are formed the cluster frequency decreases. The effect of local mean solids concentration is more complex, since a higher solids concentration, on the one hand, increases the tendency of forming more clusters; but on the other hand higher solids concentration also increases the cluster size, while reducing the number of clusters.

The radial profiles of the cluster frequency, f_c, are shown in Fig. 5 for different operating conditions. The cluster frequency is seen to increase along the radial direction, forms a peak at one point and then decreases towards the wall. The cluster frequency is low in the core region because fewer clusters are present given its dilute conditions. The decrease of the cluster frequency near the wall can be attributed to the increased size of clusters due to the increased solids concentration. The peak appears to coincide with the core–annulus interface, resulting from strong gas–solid interactions, so that aggregates form and break more frequently compared to the either the core or the annular regions. Such peaks are higher in the bottom region of the riser, indicating more gas–solid interaction there. On the other hand, in both the core and annular regions, cluster frequency increases with axial elevation, due to the reduced cluster size with decreasing solids concentration associated with solids acceleration.

The effects of the gas velocity and solids circulation rate on the cluster frequency are more complex (see Fig. 5).

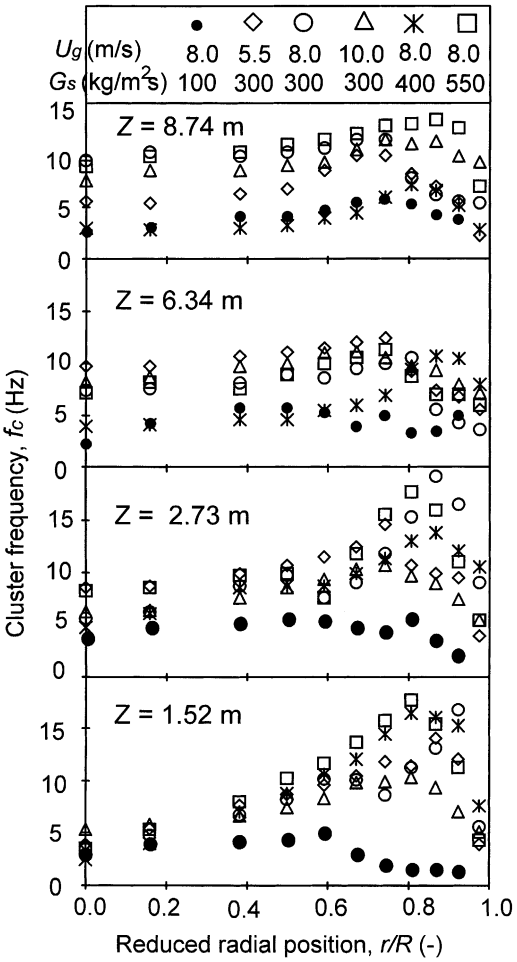

Fig. 5. Radial profiles of cluster frequency for different operating conditions and axial elevations.

Fig. 6 re-plots those frequency values against the local mean solids concentration, showing the relationship for the whole cross-section ($0 < r/R < 1.0$) and for the core region only ($0 < r/R < 0.8$). Over the whole riser cross-section, the cluster frequency increases towards a maximum before

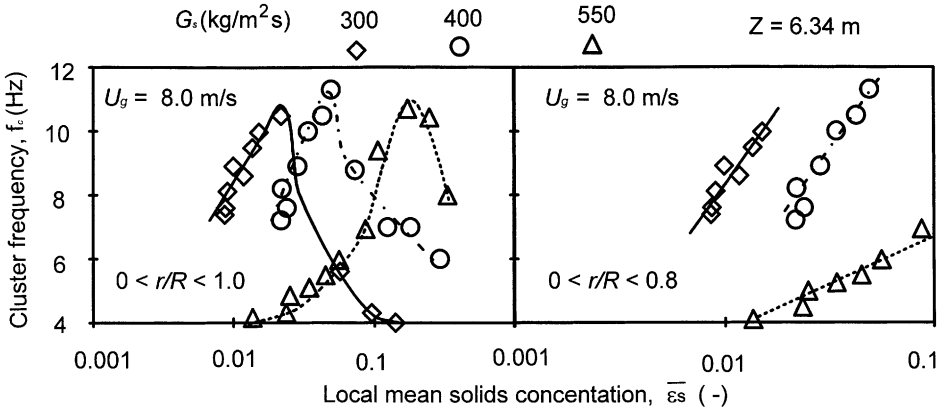

Fig. 6. Variation of local cluster frequency with the local mean solids concentration at different operating conditions in the fully developed section ($Z = 6.34$ m).

decreasing again with further increase in the solids concentration. Increasing overall solids circulation rate, G_s, moves the peak to a higher solids concentration value. In the core region, the cluster frequency increases with solids concentration without a peak, under all solids circulation rates, but a lower cluster frequency appears for high solids circulation rates due to increased solids concentration inside the clusters. Comparing the two plots, it can be seen that the decrease in the cluster frequency at higher solids concentration (after the peak) corresponds to the dense conditions near the wall. This can be attributed to the formation of large clusters near the wall and therefore few clusters in the annular region.

To further analyze the cluster frequency, clusters are classified into two groups by their existence times with a demarcation at $\bar{\tau}_c = 15$ ms, which corresponds to the maximum value of cluster existence time in the core region for all operating conditions and axial elevations. Using this classification, the frequency f_{c1} (for $\bar{\tau}_c < 15$ ms) and f_{c2} (for $\bar{\tau}_c \geq 15$ ms) are shown in Fig. 7, along with the overall frequency, f_c, for $U_g = 8.0$ m/s and $G_s = 550$ kg/m^2 s. Such analysis shows the relative distribution (frequency) of the larger clusters in the annular region and has not been reported in any previous literature. The results show that the number of larger clusters (with existence time longer than 15 ms) is comparable to the number of smaller clusters (with existence time shorter than 15 ms). With increasing axial elevation, f_{c2} decreases showing that the range of existence time narrows with axial elevation. Similarly, the overall frequency, f_c, also decreases with axial elevation. This information is very useful for the understanding of the CFB systems. For example, it provides important information for the estimation of heat and mass transfer coefficients [9].

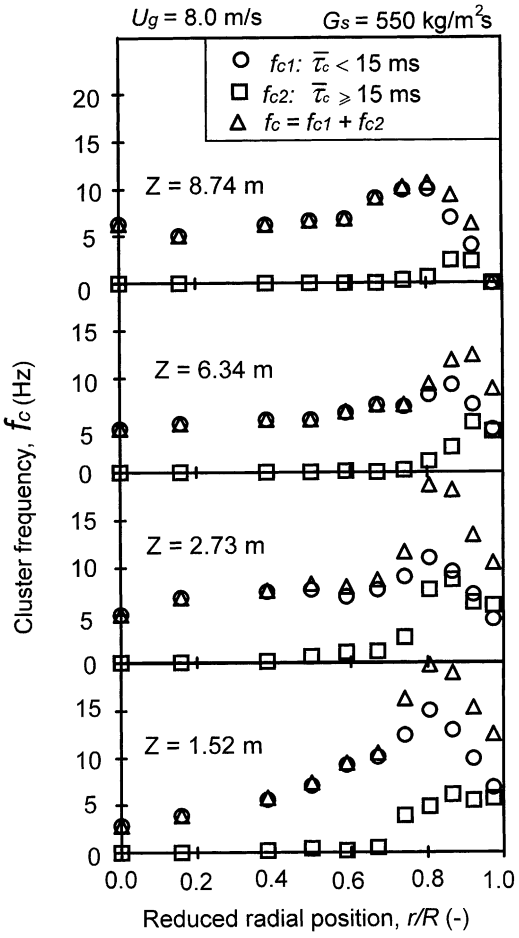

Fig. 7. Radial profiles of cluster frequencies, f_{c1}, f_{c2}, and f_c, at $U_g = 8.0$ m/s and $G_s = 550$ kg/m^2 s.

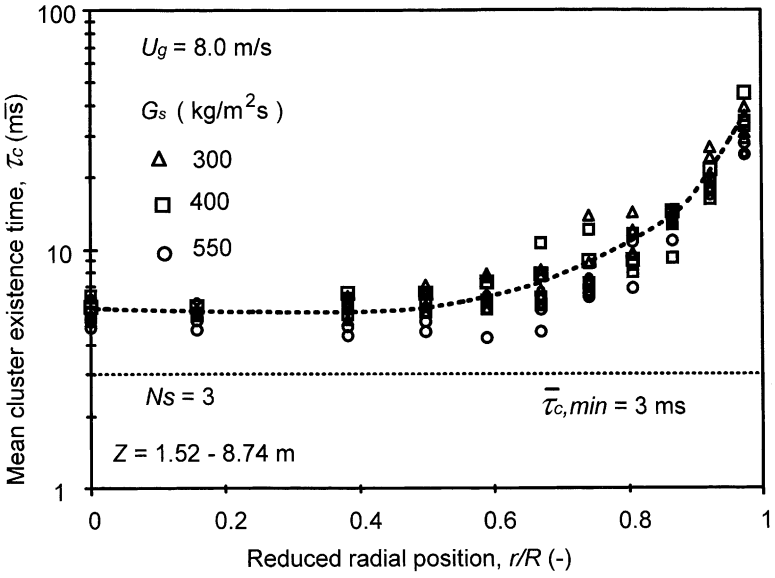

Fig. 8. Radial profiles of mean cluster existence time at $U_g = 8.0$ m/s and different solids circulation rates (data from all axial elevations).

4.4. Cluster existence time

As has been shown above, cluster existence time is an important property of clusters. In this study, the existence times for the clusters were sorted from the solids concentration signals to form a new time series, which were then further analyzed using statistics and probability for the local existence time distribution (LETD). Fig. 8 shows the radial profiles of the mean cluster existence time, $\bar{\tau}_c$, under different operating conditions and over several axial elevations. It shows that all profiles are flat and consistent with each other inside the core region. In the annular region, on the other hand, a much wider range of cluster existence time exists indicating the variation of the cluster properties with the operating conditions and axial elevation. Such a wide variation of $\bar{\tau}_c$ near the wall has been also reported by others [13].

The variation of existence time with the local mean solids concentration at different operating conditions and several axial elevations in the annular region ($r/R > 0.7$) was further studied at high-flux conditions, as shown in Fig. 9. The cluster existence time is seen to depend strongly on the average local solids concentration, increasing with increasing solids concentration for all operating conditions and axial elevations. In addition, two distinct sections are shown in this plot, where the relationship between the mean cluster existence time and the mean solids concentration in the top section of the riser ($Z > 6.0$ m) is quite different from that in the bottom section of the riser ($Z < 3.0$ m).

The variation in the local existence time for different operating conditions was also studied using the LETD, at $Z = 6.34$ m. Fig. 10 shows the strong dependency of the LETD on the radial distance from the center and on the operating conditions. While all plots show a single peak near the lowest existence time, the span of existence times in the core region is shorter compared to the wall region, due to the high gas velocity and lower solids concentration. This again indicates strong gas–solid interactions and more solids activities in the annular region.

4.5. Solids concentration inside clusters

Fig. 11 shows the radial profiles of the average solids concentration inside clusters at different operating conditions in the developed flow section ($Z = 6.34$ m). The profiles are flat in the core and increases towards the wall, similar to the time-averaged solids concentration. Comparing with Fig. 2, it is clear that higher $\bar{\varepsilon}_s$ leads to higher $\bar{\varepsilon}_{sc}$ and vice versa. Therefore, higher G_s also leads to higher $\bar{\varepsilon}_{sc}$ as observed already for $\bar{\varepsilon}_s$. The low-flux condition ($U_g = 8.0$ m/s and $G_s = 100$ kg/m^2 s) leads to correspondingly lower solids concentration inside the clusters. A strong similarity between the radial profiles of local mean solids concentration and the average solids concentration in clusters has been reported in literature [19]. Table 2 shows that our results fall

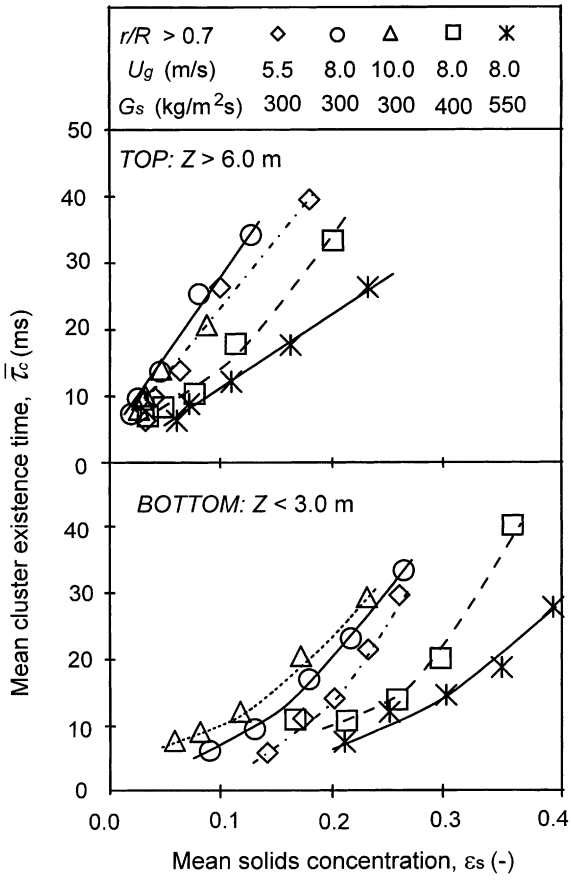

Fig. 9. Variation of mean cluster existence time with local mean solids concentration in the annular region ($r/R > 0.70$) at different operating conditions for the bottom dense section and the top dilute section of the riser.

Table 2
Literature data on the average solids concentration in clusters

References	$\bar{\varepsilon}_{sc}$	Operating conditions	Solids properties
Li et al. [4]	0.5 ($=1-\varepsilon_{mf}$)	–	$d_p = 54\,\mu$m, $\rho_p = 930$ kg/m^3
Bi et al. [2]	0.05–0.30 for streamers and strands; $\bar{\varepsilon}_{sc} = 1 - \varepsilon_{mf}$ for clusters	–	FCC catalyst
Horio et al. [17]	0.3–0.2	$U_g = 1.17$ m/s, $G_s = 11.7$ kg/m^2 s	FCC catalyst
Marzochella et al. [20]	0.5 ($=1-\varepsilon_{mf}$)	–	FCC catalyst
Yerushalmi et al. [32]	0.3–0.2	$U_g = 2.2$–5.5 m/s, $G_s = 24$–195 kg/m^2 s	$d_p = 40$ and $55\,\mu$m; $\rho_p = 1666$ and 1073 kg/m^3
Rhodes et al. [33]	0.47	$U_g = 3.0$ m/s, $G_s = 50$ kg/m^2 s	FCC catalyst

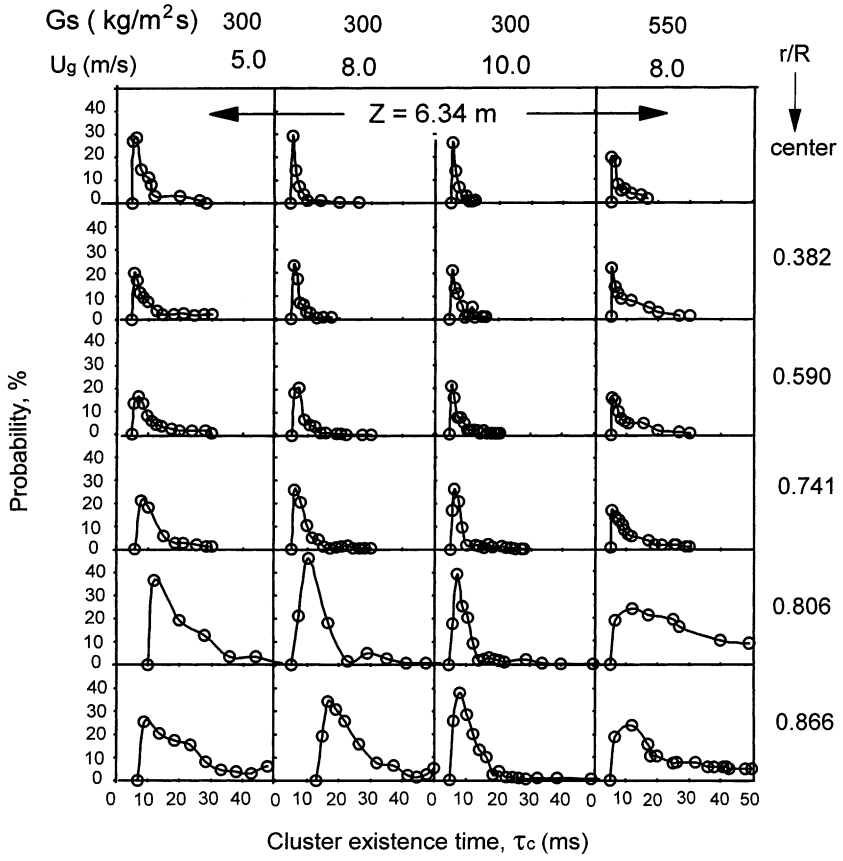

Fig. 10. Radial profiles of LETD of clusters at different operating conditions.

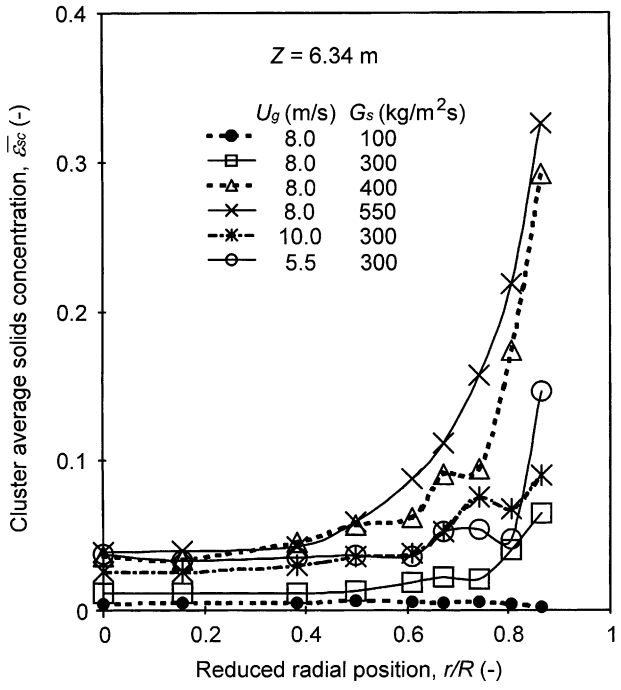

Fig. 11. Radial profiles of the mean solids concentration inside cluster at different operating conditions and $Z = 6.34$ m.

nicely in the range of the literature data for average solids concentration inside clusters, which range from as low as 0.05 for very dilute conditions [2] to as high as 0.50 for denser conditions [20].

4.6. Estimation of the vertical cluster size

Using the upward local mean particle velocity and the local mean existence time of the clusters, the characteristic vertical size of clusters, L_v, was estimated. Such vertical sizes obtained under $G_s = 300\,\text{kg/m}^2\,\text{s}$ and various U_g are plotted versus the mean cluster solids concentration in Fig. 12. It is interesting to note that the vertical length can reach nearly 100 mm, which is about 1500 times of the 67 μm average particle size. The characteristic length decreases with increasing solids concentration inside the clusters for all operating conditions. At the top of the riser, the characteristic size depends only on the cluster solids concentration and does not change with gas velocity. At $Z = 2.73$ m, the characteristic length is comparably low, despite the dense conditions, probably due to intensive refluxing of solids at this level. The effect of gas velocity is not clear. Streamer lengths of 5–50 mm (depending on gas velocity) and cluster sizes between 5 and 30 mm have been observed in risers [2,17].

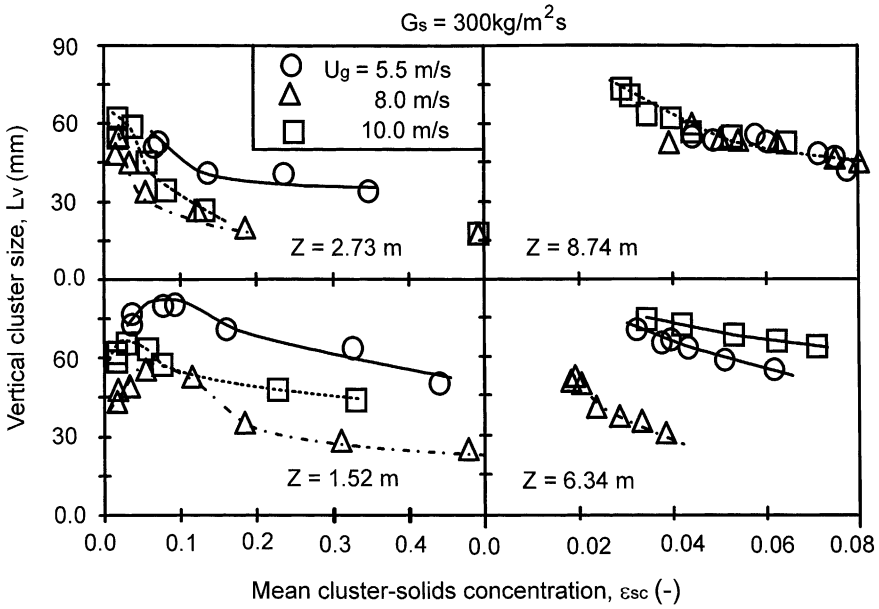

Fig. 12. Variation of characteristic vertical cluster size with mean cluster solids concentration, in the core region of the riser at $G_s = 300\,kg/m^2\,s$ for different gas velocities and axial elevations.

Table 3
Summary of results for cluster properties between core and annulus

Cluster properties	Core	Annulus
Time-averaged solids concentration, $\bar{\varepsilon}_s$	Flat profiles without distinction between operating conditions; lower solids concentration	Increases fast near the wall depending on axial elevation; clear effect of operating conditions at higher elevations
Cluster time fraction	Lower; relatively flat profiles at higher elevations; depends on operating conditions	Higher; depends strongly on axial elevation and operating conditions; very sharp increase towards the wall for higher G_s
Cluster frequency	Increases with r/R; depends on operating conditions and axial elevation	Decreases towards the wall; depends on operating conditions and axial elevation
Local mean cluster existence time	Shorter existence times; depends on operating conditions and axial elevation; relatively flat profiles	Longer existence times; increases fast towards the wall; strongly depends on operating conditions

Table 3 summarizes the radial profiles of cluster properties from this study. It can be seen that the cluster properties depend strongly on the radial position.

5. Conclusion

Using the measurements of transient solids concentration obtained via a fiber optic probe, the cluster properties were studied in a riser operated at high-flux conditions. A sensitivity analysis shows that the cluster properties depends strongly on the set parameters n and N_s, and determines the optimum values of these two parameters. A wide range of cluster properties, time fraction, frequency, existence time, average solids concentration and vertical size have been studied. Using the average local existence time and the average particle velocity, the vertical sizes of clusters were also estimated. The following conclusions can be made from this work:

1. These cluster properties depend strongly on the local mean solids concentration, axial and radial positions and the operating conditions.
2. The cluster time fraction range between 0 and 15% in the core and from 15 to 30% near the wall for high-flux operating conditions, while low-flux conditions show comparable results in the core but lower values near the wall.
3. Highest cluster frequency exists at the interface between the core and the annulus. The frequency is lower in the core compared to the region near the wall. The frequency of clusters with existence times longer than 15 ms is nearly zero in the core.
4. Near the wall, the average existence time of clusters varies from 3 to 50 ms; while in the center, only between 3 and 15 ms. Existence time of clusters increases faster near the wall where clusters exist up to 50 ms on average.
5. The vertical sizes of the clusters range up to 1500 times of the particle diameter under high-flux conditions.

Acknowledgements

The authors are grateful to the NSERC for the financial support to the work presented in this paper. S.V. Manyele

would also like to thank NORAD-UDSM for a scholarship to study at UWO.

References

[1] Y. Li, M. Kwauk, The dynamics of fast fluidization, in: J.R. Grace, J.M. Matsen (Eds.), Fluidization, Plenum Press, New York, 1980, pp. 537–544.
[2] H.T. Bi, J. Zhu, Y. Jin, Z.-Q. Yu, Forms of particle aggregations in CFBs, in: Proceedings of the Sixth Chinese Conference on Fluidization, Wuhan, China, 1993, pp. 162–167.
[3] J.R. Grace, J. Tuot, A theory for cluster formation in vertically conveyed suspension of intermediate density, Trans. IChemE 57 (1979) 49–54.
[4] J. Li, Y. Tung, M. Kwauk, Method of energy minimization in multi-scale modeling of particle–fluid two-phase flow, in: P. Basu, J.F. Large (Eds.), Circulating Fluidized Bed Technology II, Pergamon Press, Toronto, 1988, pp. 89–103.
[5] Y. Fujima, K. Tagashira, Y. Tagahashi, S. Ohme, S. Ichimura, Y. Arakawa, Conceptual study on fast fluidization formation, in: P. Basu, M. Horio, M. Hasatani (Eds.), Circulating Fluidized Bed Technology III, Pergamon Press, Toronto, 1991, pp. 85–90.
[6] F. Wei, Y. Jin, Z.-Q. Yu, The visualization of macro structure of gas–solid suspension in circulating fluidized beds, in: A.A. Avidan (Ed.), Circulating Fluidized Bed Technology IV, AIChE, New York, 1994, pp. 588–593.
[7] M. Horio, H. Kuroki, Three-dimensional flow visualization of dilute dispersed solids in bubbling and circulating fluidized beds, Chem. Eng. Sci. 49 (1994) 2413–2421.
[8] R. Bader, J. Findlay, T.M. Knowlton, Gas/solid flow patterns in a 30.5 cm diameter circulating fluidized bed, in: P. Basu, J.F. Large (Eds.), Circulating Fluidized Bed Technology II, Pergamon Press, Oxford, 1988, pp. 123–137.
[9] L.R. Glicksman, Circulating fluidized bed heat transfer, in: P. Basu, J.F. Large (Eds.), Circulating Fluidized Bed Technology II, Pergamon Press, Oxford, 1988, pp. 13–29.
[10] E.-U. Hartge, D. Rensner, J. Werther, Solids concentration and velocity patterns in circulating fluidized beds, in: P. Basu, J.F. Large (Eds.), Circulating Fluidized Beds Technology II, Pergamon Press, Oxford, 1988, pp. 165–180.
[11] J.H. Pärssinen, P. Hagelberg, I. Eilos, J. Aittamaa, Application of dynamic pressure probe technique to characterize a circulating fluidized bed, Can. J. Chem. Eng. 77 (1999) 229–304.
[12] B. Zethræus, B. Ljungdahl, A first approach to the development and behavior of particle aggregates in the central part of a CFB riser, in: A.A. Avidan (Ed.), Circulating Fluidized Bed Technology IV, AIChE, New York, 1994, pp. 628–634.
[13] C.H. Soong, K. Tuzla, J.C. Chen, Identification of particle clusters in circulating fluidized bed, in: A.A. Avidan (Ed.), Circulating Fluidized Bed Technology IV, AIChE, New York, 1994, pp. 615–620.
[14] C.H. Soong, K. Tuzla, J.C. Chen, Experimental determination of cluster size and velocity in circulating fluidized bed, in: J.F. Large, C. Laguerie (Eds.), Fluidization VIII, Engineering Foundation, New York, 1995, pp. 219–227.
[15] U. Lackermeier, C. Rudnick, J. Werther, A. Bredebusch, H. Burkhardt, Visualization of flow structures inside a circulating fluidized bed by means of laser sheet and image processing, Powder Technol. 114 (2001) 71–83.
[16] H. Hatano, H. Takeuchi, S. Sakurai, T. Masuyama, K. Tsuchiya, Motion of individual FCC particles and swarms in a circulating fluidized bed riser analyzed via high speed imaging, AIChE Symp. Ser. 318 (94) (1998) 31–36.
[17] M. Horio, K. Morishita, O. Tachibana, N. Murauta, Solid distribution and movement in circulating fluidized beds, in: P. Basu, J.F. Large (Eds.), Circulating Fluidized Beds Technology II, Pergamon Press, Toronto, 1988, pp. 147–154.
[18] B. Zou, H. Li, Y. Xia, X. Ma, Cluster structure in a circulating fluidized bed, Powder Technol. 78 (1994) 173–178.
[19] H. Li, Y. Xia, Y. Tung, M. Kwauk, Micro-visualization of clusters in a fast fluidized bed, Powder Technol. 66 (1991) 231–235.
[20] A. Marzochella, U. Arena, A. Cammarota, L. Massimilla, Breakup of cylindrical clusters of solid particles under gravity flow in a two dimensional columns, Powder Technol. 65 (1991) 453–460.
[21] D. Subbarao, Clusters and lean-phase behaviour, Powder Technol. 46 (1986) 101–107.
[22] M. Fligner, P.H. Schipper, A.V. Sapre, F.J. Krambeck, Two-phase cluster model in riser reactors: impact of radial density distribution on yields, Chem. Eng. Sci. 49 (1994) 5813–5818.
[23] J.J. Nieuwland, P. Huizenga, J.A.M. Kuipers, W.P.M. van Swaaij, Hydrodynamic modelling of circulating fluidized beds, Chem. Eng. Sci. 49 (1994) 5803–5811.
[24] O. Iodarche, Y. Bloise, J. Choauki, R. Legross, Clusters in circulating fluidized beds: kinetic theory approach, Chem. Eng. Commun. 131 (1995) 53–71.
[25] Y. Tsuji, T. Tanaka, S. Yonemura, Cluster patterns in circulating fluidized beds predicted by numerical simulation (discrete particle model versus two-fluid model), Powder Technol. 95 (1998) 254–264.
[26] A.F. Fortes, P. Caldas, J.V. Gallo, Particle aggregates and the van der Waals forces in gas–solids fluidization, Powder Technol. 98 (1998) 201–208.
[27] J. Zhu, H.T. Bi, Distinctions between low density and high density circulating fluidized beds, Can. J. Chem. Eng. 73 (1995) 644–649.
[28] J.H. Pärssinen, J.-X. Zhu, Solids Concentration and Flow Development in a Long High Flux Circulating Fluidized Bed Riser, AIChE J. 47 (2001) 2197–2205.
[29] H. Zhang, P.M. Johnston, J.-X. Zhu, H.I. de Lasa, M.A. Bergougnou, A novel calibration procedure for a fiber optic concentration probe, Powder Technol. 100 (1998) 260–272.
[30] J.-X. Zhu, G.-Z. Li, S.-Z. Qin, F.-Y. Li, H. Zhang, Y.-L. Yang, Direct measurements of particle velocities in a circulating fluidized bed using a novel optical fiber probe, Powder Technol. 115 (2001) 184–192.
[31] K. Tuzla, A.K. Sharma, J.C. Chen, T. Schiewe, K.E. Wirth, O. Molerus, Transient dynamics of solids concentration in downer fluidized bed, Powder Technol. 100 (1998) 166–172.
[32] J. Yerushalmi, N.T. Cankurt, D. Geldart, B. Liss, Flow regimes in vertical gas–solid contact systems, AIChE Symp. Ser. 74 (176) (1978) 1–12.
[33] M.J. Rhodes, T. Hirama, G. Cerutti, D. Geldart, Nonuniformity of solids flow in the risers of circulating fluidized beds, in: J.R. Grace, L.W. Shemilt, M.A. Bergougnou (Eds.), Fluidization VI, Engineering Foundation, New York, 1989, pp. 73–80.